Influence of powder nitriding on the mechanical behavior of laser-powder bed fusion processed tool steel X30CrMo7-2

Felix Stern, Felix Grabienski, Frank Walther, Dortmund, Johannes Boes, Arne Röttger and Werner Theisen, Bochum, Germany

Additive manufacturing allows for the production of highly complex structures due to its layer-wise local melting of powder material. For this reason, this technique has a high potential for manufacturing extremely lightweight components potential. However, laser based additive manufacturing is still restricted due to the limited amount of processable alloys, especially Fe-based materials. A main object in current research is to expand the varieties for steel that may be used. Additionally, the modification and optimization of steel powder is seen as an interesting aspect for improving the material properties of additively manufactured parts. In this work, secondary hardenable martensitic tool steel X30CrMo7-2 is investigated, starting from the raw powder which is enriched with nitrogen by gas nitriding and subsequently characterized to ensure the usability of the modified powder for laser-powder bed fusion. In a next step, the raw and nitrided powder are used to generate cylindrical specimens to allow for further analysis of the microstructure and for a mechanical characterization of compression behavior. Moreover, a variety of heat treatments is carried out. The higher content of nitrogen leads to an increase in porosity. However, the addition of nitrogen causes an increase in hardness and in the compressive yield point, especially after heat treatment. After tempering, compressive yield stress is increased from 1,111 MPa to 1990 MPa, while for conventional material it is slightly reduced from 1,316 MPa to 1225 MPa.

Article Information

Correspondence Address
Felix Stern
Department of Materials Test Engineering (WPT)
TU Dortmund University
Baroper Str. 303
D-44227 Dortmund
Germany
E-mail: felix.stern@tu-dortmund.de

Keywords
Powder modification, gas nitriding, tool steel, laser-powder bed fusion, compression test

The possibility of creating near net shape parts by using additive manufacturing (AM) processes, here the laser-powder bed fusion (L-PBF) of metallic materials, has gained a lot of interest from researchers as well as various industries such as the automotive and aviation branches. The high flexibility of the process allows for the production of components directly from a 3D CAD model with almost no limits regarding geometrical complexity. However, AM is not only still limited due to poor surface quality and process-induced defects such as lack of fusion and gas porosity but also because of a very limited amount of available material which can be successfully processed. The most common materials used for L-PBF are aluminum (AlSi12, AlSi10Mg) and titanium alloys (TiAl6V4). Further investigations are focused on Fe-based alloys such as austenitic stainless steel (e. g. 316L/304L) and other alloys, mainly maraging steel (18Ni-300), and tool steel (H13) [1].

One of the essential aspects for L-PBF applications is the use of the powder needed as a raw material. In this state, the material has an advantage that it can be directly modified to influence or enhance the material behavior at a later product. The modification of powder for AM was already performed by Gu et al. [2] for a Ti-Al matrix composite by mechanically alloying Ti-Al-graphite elemental powder for L-PBF. In this way, it was possible to form TiC nano particles in situ. Mechanical alloying was also employed by AlMangour et al. for the H13 steel [3] used to implement TiC-nano particles in order to achieve greater hardness and an increased elastic modulus. Ad-

sorption of Al_2O_3-nanoparticles onto the surface of the powder particles was performed by Sehrt et al. [4] for a Ni-based alloy and a tool steel resulting in increased hardness for both materials.

Another approach was realized by Doñate-Buendía et al. [5]. Here, the powder was electrochemically decorated with Y_2O_3-nanoparticles to produce an oxide dispersion-strengthened Fe-based powder for manufacturing parts by laser metal deposition (LMD) for high temperature application. An interesting approach for implementing nitrides and oxides in materials was carried out by Springer et al. [6] by using nitrogen and oxygen containing atmospheres during LMD and the arc-welding of an austenitic stainless steel.

However, to the authors' knowledge, no nitriding of steel powder for AM application has been performed yet. It is known that the addition of nitrogen to Fe-based alloys has several advantages. The effect ranges from a more effective means in solution strengthening and grain refinement as compared to that of carbon [7] to the replacement of nickel due to its austenite-forming and -stabilizing influence [8, 9] for improving strength, toughness [9, 10] and corrosion resistance [11, 12]. Specific alloys with a nitrogen content of up to 1 wt.-%, where corrosion resistance and bio-compatibility are necessary, are of great interest for medical applications [13]. Duan et al. [14] increased the amount of nitrogen in two similar stainless steel powders for sintering applications by means of mechanical alloying in a nitrogen atmosphere and by adding chromium nitride powder [15]. Steel parts (AISI 4130) constructed by L-PBF were then plasma-nitrided by Nakamoto et al. [16] to create a hardened compound layer on the surface of the specimen and resulting in improved wear resistance.

In this study, tool steel X30CrMo7-2 in the form of powder is gas-nitrided to achieve an increased amount of nitrogen. The resulting powder is characterized in terms of the processability for L-PBF and subsequently densified. Additionally, two different heat treatments are used. The resulting microstructures are compared to that of the raw material, and process-induced defects are achieved by 3D non-destructive micro-focus computed tomography (µ-CT). Furthermore, micro-hardness measurements and quasistatic compression tests are used to determine the influence of the increased nitrogen content on the material properties.

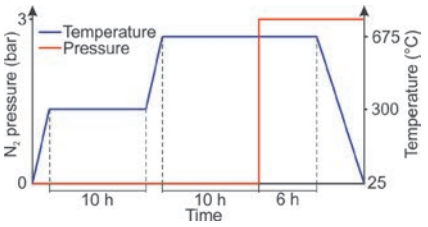

Figure 1: Process parameters for gas nitriding of raw steel powder

Material and manufacturing process

Investigated material. The investigated tool steel X30CrMo7-2 (SZW5051) was delivered by DEW Deutsche Edelstahlwerke Specialty Steel GmbH & Co. KG (Germany). The chemical composition of the received powder is listed in Table 1. The material used is a martensitic hardenable filler material, possessing good weldability, which is an important characteristic for using the alloy in laser based additive manufacturing processes.

Thermodynamic equilibrium calculations. For an approximate estimation of the nitrogen content after nitriding and in order to gain a deeper understanding of the microstructure formation during nitriding, thermodynamic equilibrium calculations were performed. Calculations based on the CALPHAD method were carried out using ThermoCalc® software (Thermo-Calc Software AB, Sweden) with thermodynamic data taken from TCFe9 database. In the simulations, a system size of 1 mole, a nitrogen pressure of 3 bar and a temperature of 675 °C was inspected.

Nitriding process. In order to adjust the nitrogen content of the steel powder investigated, the powder was gas-nitrided. The nitriding process was performed using a vacuum furnace type IU 54/1F from Schmetz GmbH (Germany). As nitrogen donor N_2 gas was used. During the nitriding process, a temperature of 675 °C and a nitrogen pressure of 3 bar were applied. Before increasing the nitrogen pressure, the furnace was evacuated and the temperature was raised stepwise, as depicted in Figure 1. The temperature and pressure control were chosen based on previous investigations of the nitriding of steel powder for significantly reducing powder oxidation.

Laser-powder bed fusion. All specimens were manufactured on a SLM 100 System (ReaLizer GmbH, Germany) equipped with an Ytterbium fiber laser with a wavelength of λ = 1075.5 nm, a focal spot size of ~90 µm and a nominal output power of 100 W (effective output power of P_{eff} = 77.4 W). Argon was used as a shielding gas to prevent oxidation during the manufacturing process. The oxygen content inside the build chamber was kept below 0.3 vol.-%.

Both batches were manufactured using identical process parameters as listed in Table 2. As follows from Equation (1), the laser parameters used result in a line energy density of 258 J × m^{-1} with P_d as the point distance (µm) and t_e as the exposure time (µs). The only difference was the use of raw powder for the L-PBF of batch A and nitrided powder for batch B. The hatch orientation alternated by 90° in consecutively built slices. For microstructural and mechanical investigations, cylindrical samples with a diameter of 4 mm and a height of 6 mm and an additional support structure to connect the samples with the build platform were built for each batch.

$$E_l = \frac{P_{eff}}{\frac{p_d}{t_E}} \quad (1)$$

Heat treatment. The cylindrical samples were heat treated following two different heat treatment concepts. Based on previous findings on L-PBF-built martensitic secondary hardenable tool steels, both quenching and tempering or solely the tempering of the L-PBF-built steel were identified as pos-

C	Si	Mn	P	S	Cr	Mo	N	O	Al	Fe
0.33	0.34	0.78	0.013	0.009	6.93	2.26	0.049	0.028	<0.005	bal.

Table 1: Chemical composition of raw tool steel powder X30CrMo7-2 as provided by the powder manufacturer (mass-%)

Batch	Hatch distance (µm)	Point distance (µm)	Layer thickness (µm)	Exposure time (ms)	Process atmosphere	Nitrided powder
A	120	30	30	100	Argon	–
B						yes

Table 2: Process parameters for L-PBF of X30CrMo7-2

sible heat treatments for the production of a tempered and secondary hardened martensitic microstructure [17, 18]. For the investigated steel, previous investigations revealed a shift in the secondary hardness peak in the direction of higher tempering temperatures comparing conventionally (peak at ~550 °C) and L-PBF-produced samples (peak at ~520 °C). In accordance with these findings, the heat treatment parameters for the samples built in this work were chosen as listed in Table 3.

Experimental setup

Powder characterization. The steel powder investigated was characterized with respect to its chemical composition, flow time, bulk density and packing density. Both, untreated and nitrided powder were investigated, focusing on the influence of the nitriding process on the powder properties. For a characterization of the flowability of the powders, the flow time was determined using a Hall flowmeter. Measurements were performed in accordance with DIN EN ISO 4490. Furthermore, the bulk density of the powders was measured according to standard DIN ISO 697, and the packing density was calculated with respect to the theoretical density of the steel investigated. Through scanning electron microscopy (SEM) investigations using an SEM type MIRA 3 from Tescan (Czech Republic) with an acceleration voltage of 15 kV and a working distance of 15 mm, the particle morphology and microstructure were characterized. Additionally, the nitrogen and oxygen content of the powder in initial and nitrided condition were measured by carrier gas hot extraction using an ONH-200 analyzer instrument from ELTRA GmbH (Germany).

Microstructure analysis. The specimens obtained, made by L-PBF manufacturing, were hot-embedded for microstructural characterization. Longitudinal and transversal cuts were ground and polished with a diamond suspension (6 µm, 3 µm and 1 µm) and oxide polish suspension (0.25 µm). To reveal the process-induced melt pools and microstructure, the samples were etched and investigated using an Axio Imager optical microscope (OM) and SEM. Hardness measurements were performed at the longitudinal cross section of the cylindrical specimens. Vickers hardness with a load of 0.1 g (0.9807 N; HV0.1) according to DIN EN ISO 6507-1 was measured with a Shimadzu DUH-211-E hardness tester (Japan).

Computed tomography analysis. The non-destructive 3D-characterization of the process-induced porosity was conducted by using X-ray microfocus computed tomography (µ-CT). The µ-CT analyses was performed on a Nikon XT H 160 system (Nikon, Japan) equipped with a microfocus X-ray source, which can reach a maximum acceleration voltage of 160 kV. The steel samples were scanned at an acceleration voltage of 160 kV and an exposure time of 250 ms, including their support structure as shown in Figure 2a prior to the preparation for the mechanical characterization.

For each batch, one specimen in the as-built condition was scanned, reconstructed and subsequently loaded into the analyzing and visualizing software VGStudio Max 3.2 (Volume Graphics GmbH, Germany). By using the so-called algorithm "VGEasyPore", specific voxels can be characterized as defects based on their grey value and a defined local threshold for contrast.

Compression tests. For mechanical testing, quasistatic compression tests at room temperature for the evaluation of deformation behavior according to DIN 50106 were carried out on a servohydraulic testing system (Instron PSB100, Instron 8800 Controller, Instron, USA) with a 100 kN load cell. The cylindrical specimens, manufactured and used in this work, are shown in Figures 2a and 2b. To minimize friction between specimen and compression dies the end face surfaces of the specimens were smoothed and polished down to $R_z \leq 1.6$ µm, resulting in a reduced height of 5 mm (see Figure 2b). Additionally, the faces were greased with lubricant. The shell surface of the cylinders was not further modified, and thus left in the as-built state. The compression dies were made of tungsten carbide-cobalt hard metal (WC-Co). Before testing the specimens were adjusted using a device to prevent misalignment.

Compression was measured via a tactile extensometer applied at the WC-Co compression dies above and below the specimen. The tests were conducted at a controlled deformation rate of $e_{d1} = 2.3 \times 10^{-3}$ mm × s^{-1} up to a displacement of 0.2 mm which was increased to $e_{d2} = 0.4 \times 10^{-1}$ mm × s^{-1} up to a maximum deformation of 2.0 mm. For every batch, three specimens were tested. The applied load was parallel to the building direction (BD) in L-PBF.

Results and discussion

Powder characterization. In the initial condition, the powder particles mostly reveal a spherical shape and only small amounts of satellites can be found. At the surface of the particles, fine dendritic structures can be observed (see Figures 3a and 3c).

The particle microstructure is characterized by a needle-like morphology as seen in Figure 4a, indicating the presence of phase α'-martensite. In addition to martensite needles, micro-segregations are also detectable in the particles. The presence of the segregations can be accounted to the high cooling and associated solidification rates occurring during gas atomization [19].

In the initial condition, the powder possess a nitrogen content of 0.049 wt.-%. In the course of the nitriding process, the steel powder is heated up to 675 °C and an N_2 pressure of 3 bar is applied. Due to these conditions, the steel powder undergoes various changes concerning the particle microstructure and the chemical com-

Heat treatment condition	Quenching parameters	Tempering temperature
Tempered (T)	–	590 °C (2 × 2 h)
Quenched and tempered (QT)	T_{Aust} = 1000 °C, t_{Aust} = 20 min, quenching medium: Oil	575 °C (2 × 2 h)

Table 3: Heat treatment parameters used

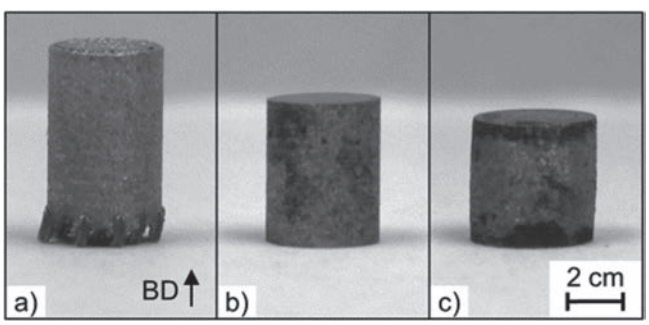

Figure 2: Cylindrical specimens a) after L-PBF process; b) after removal of support structure and polishing of the faces; c) after compression test

position. The nitrogen content of the powder is increased to 0.68 wt.-% after nitriding. Based on thermodynamic equilibrium calculations, the nitrogen uptake during the nitriding process is accompanied by the formation of M(C,N) carbonitrides and Fe_3C as listed in Table 4.

Furthermore, the metallic matrix reveals a cubic body-centered crystal structure in equilibrium conditions. With respect to the calculations, a nitrogen content of 1.9 wt.-% is soluble in the investigated steel at the given temperature and pressure. Taking the nitrogen content of the respective phases into account, a large part of the nitrogen take-up is due to the formation of considerable amounts of nitrogen-rich Cr-based carbonitrides. In accordance with the simulations, cross-sections of nitrided powder particles exhibit precipitates with a chemical composition corresponding to the predicted M(C,N) precipitates (see Figure 4b).

However, the amount of carbonitrides in the nitrided powder is significantly lower than the calculated amount, which indicates, that the nitriding time of 6 h was too short for the system to reach thermodynamic equilibrium. The calculations performed do not take the local element distribution and diffusion phenomena into account, thus overestimating the fraction of M(C,N) precipitates in the powder particles. In the nitriding process, the diffusion of alloying elements is necessary for the formation of nitrogen rich phases. For this reason, carbonitrides can be mainly found at the outer parts of the powder particles, which corresponds to the diffusion paths of nitrogen into the powder particles. While larger particles do not show precipitates in the complete cross-section, in smaller particles, the diffusion distances of nitrogen under the given conditions were sufficient for the formation of carbonitride over the entire cross-section.

Another reason for the higher calculated nitrogen content as compared to the nitrogen content measured is that the calculations performed do not take into account the thermal dissociation rate of nitrogen gas at the respective temperature and assume the availability of atomic nitrogen. In the nitriding procedure conducted however, nitrogen is present as N_2 molecules and, on the basis of literature, the thermal dissociation rate has to be considered relatively low at the given temperature of 675 °C [20]. From the considerable nitrogen uptake, it can nonetheless be concluded that the low thermal dissociation rate of the process gas used is counteracted by the high specific surface of the powder particles which offer a large reaction area for nitrogen dissociation and diffusion.

Corresponding to the formation of precipitates inside the particles, fine precipitates were also observed on the surfaces of the nitrided powder particles (see Figures 3b and 3d). Moreover, some particles possess slightly flattened surface areas. Currently, these minor deformations are assumed to be induced by slight sintering of the particles during nitriding and the breakup of the resulting agglomerates during powder preparation (tumbling, mechanical sieving). Against the background of the processability of the investigated powders by means of L-PBF, a change of the particle surfaces and the particle morphology might have an influence on the powder properties. For a sufficient processability of metallic powders with L-PBF, especially good flow properties and a high packing density are necessary. As listed in Table 5, the nitriding process does not affect the overall powder properties intensely. For the use of the powders in the L-PBF device SLM 100 from Realizer GmbH, the determined flow time and packing density could be evaluated as sufficient.

Microstructure analysis. After processing the nitrided powder, it can be deter-

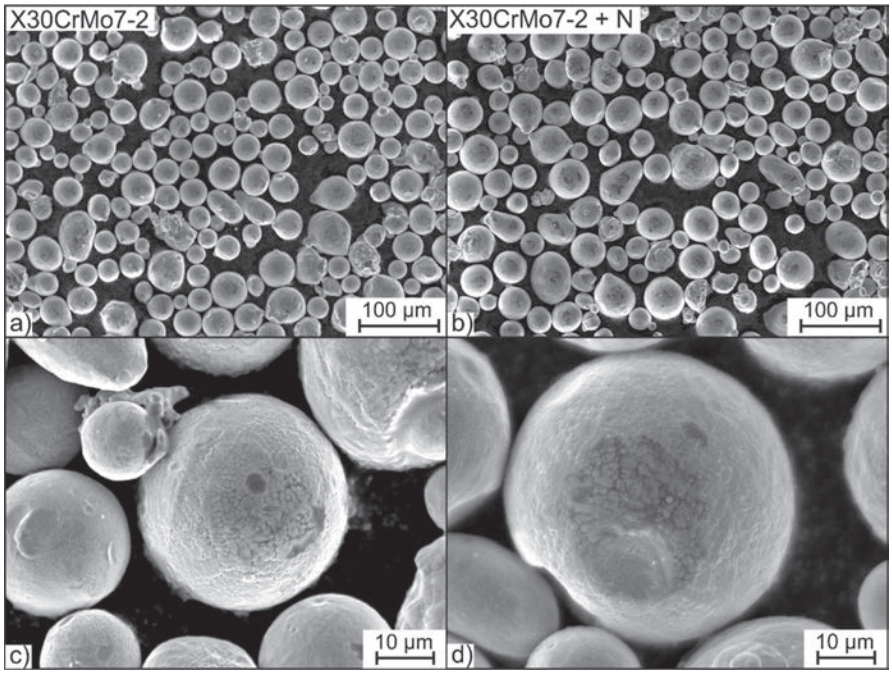

Figure 3: SEM-micrographs of powder particles in a), c) initial condition and b), d) after nitriding

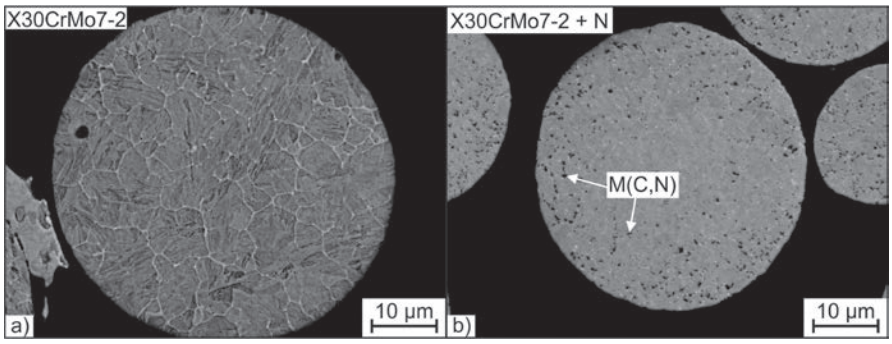

Figure 4: SEM-micrographs of etched cross-sections of powder particles in a) initial condition and b) nitrided condition

Phase	Volume fraction	N content in wt.-%
Ferrite	0.864	0.003
M(C,N)	0.130	16.58
Fe_3C	0.006	0.0002

Table 4: Volume fraction and nitrogen content of thermodynamically stable phases at a temperature of 675 °C and a N_2 pressure of 3 bar

mined that the L-PBF steel samples possess a nitrogen content of 0.47 wt.-%, indicating a degassing during L-PBF as compared to the amount of nitrogen in the nitrided steel powder. This observation is supported by the OM and SEM investigations of the samples. The defects in batch A mainly consist of a lack of fusions due to the insufficient overlap of the laser scan tracks which can be found between the single melt pools directly aligned above each other. The location of these defects can be traced back to the applied meandering scanning strategy (see Figure 5a). In Figure 5b (Batch B), gas pores with a round and more spherical shape can be found, which is an indication of the possible degassing of nitrogen during L-PBF. Due to the applied etching, the melt pools can clearly be identified in the as-built condition. After tempering (T), this holds true for the raw samples (see Figure 5c). However, for Batch B, the melt pools are barely visible but still present (see Figure 5d). Hardening (QT) results in a complete change in the microstructure (see Figures 5e and 5f), being comparable to the microstructure of additively manufactured X37CrMoV5-1 steel after quenching and tempering and leading to a homogeneous martensitic structure [21].

Additional investigations via SEM reveal not only the melt pool boundaries but also the fine dendritic microstructure after L-PBF in the as-built condition (see Figure 6a). Based on the literature, this dendritic or cellular structure is attributed to local chemical variations in the steel caused by the high cooling rates which lead to micro-segregations of heavy elements such as Mo [17]. As compared with the OM images, this structure completely changes after QT (seev Figure 6b), showing a typical needle-like morphology, again indicating the presence of α'-martensite.

The results of the hardness measurements, as listed in Table 6, show a decrease in hardness after both conducted heat treatments of the unmodified material. The hardness decrease is relatively strong (approx. 120 HV0.1), therefore indicating that the tempering temperatures were higher than the assumed secondary hardness peak of the material. However, the hardness reached is acceptable for a comparative study of the steel modification conducted. The modification of the investigated steel by the addition of nitrogen causes slightly higher hardness in the as-built condition and significantly higher hardness in the heat-treated condition as compared to the

Powder	Flow time t (s)	Bulk density ρ (g × cm^{-3})	Packing density
X30CrMo7-2	15.6	4.34	0.567
X30CrMo7-2+N	15.4	4.26	0.556

Table 5: Powder properties of the powder investigated in initial and nitrided condition

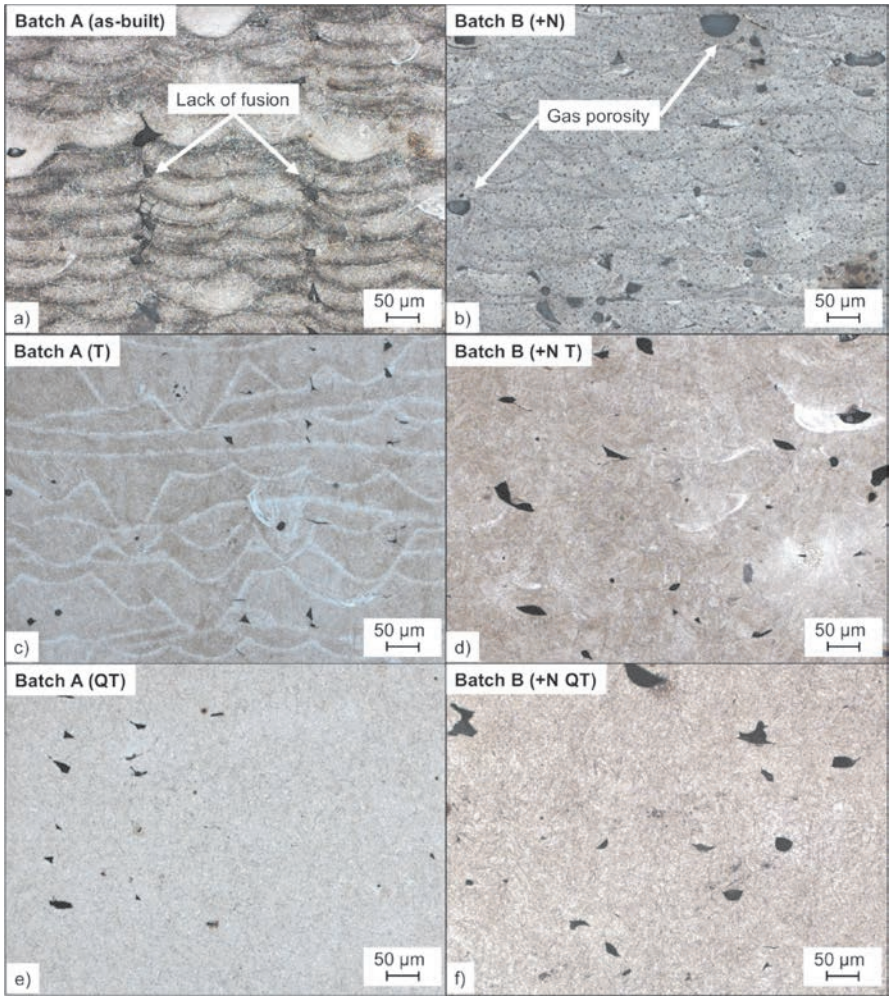

Figure 5: Microstructure of the cylindrical specimens manufactured for raw and nitrided material in a), b) as-built, c), d) tempered and e), f) quenched and tempered condition, respectively, all at an angle perpendicular to the building direction

Batch	Vickers hardness (HV0.1)		
	As-built	(T)	(QT)
A	582 ± 46	461 ± 12	458 ± 13
B	605 ± 19	724 ± 26	596 ± 7

Table 6: Results of micro-hardness measurements (HV0.1) for batch A and B

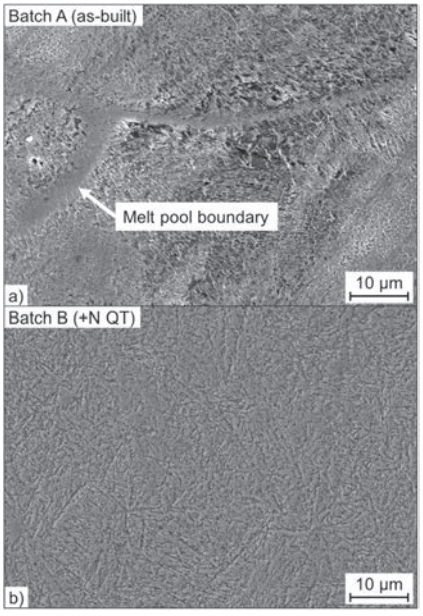

Figure 6: High magnification SEM images of the microstructure of a) the raw material in as-built condition material and b) the quenched and tempered (QT) sample with increased nitrogen (viewed perpendicular to the building direction)

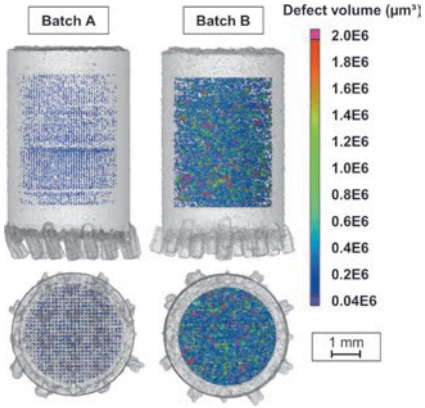

Figure 7: Results of µ-CT scans for batch A and B in side- and top-view (as-built)

unmodified material. Especially in tempered condition (T), the hardness of the material is remarkably high. This indicates a high matrix potential, resulting from the high temperatures present during L-PBF which leads to the dissolution of large parts of the alloying elements in the matrix. During tempering, a high amount of alloying elements is then available for the formation of secondary carbides, which form homogenously distributed in the presence of nitrogen [22]. Applying additional austenitization and quenching to the material counteracts the aforementioned high matrix potential by reducing the homogeneity of the element distribution in the matrix after L-PBF. In consequence, the hardness reached after quenching and tempering (QT) is significantly lower as compared to the tempered condition.

Computed tomography analysis. The 3D-volumes of the samples scanned for Batch A and B, including location and the false-color coding of the detected defects and pores based on their defect volume, can be found in Figure 7. As no difference in porosity is expected due to heat treatment, only the as-built specimens are shown here. The difference between the specimens built with and without additional nitrogen is clearly visible and in accordance with the OM and SEM images of the investigated sections. It should be mentioned that the volume analyzed is reduced to the bulk material without including the outer edge of the cylinder. In this area, an insufficient fusion of the outer rim with the inner core can be found caused by the transition region between core and contour of the sample. As the defects in this region are preventing the view inside they are not shown here.

The porosity detected shows a significant difference between Batch A and B. For Batch A, a density of 99.5 % was reached, whereas the specimen in Batch B only revealed a density of 95.6 % based on µ-CT results. Especially for Batch A, the location of the process-induced defects directly correlates with the applied scanning strategy, a phenomenon already seen in the OM images. These defects created between intersections of the scanning lines may be caused by an insufficient overlap of the melt pools. For this reason, the specific alignment of the pores, in particular in the top view, can be found.

The addition of nitrogen for Batch B leads to a vast increase in high-volume defects, again supporting the results of OM investigations. As the maximum solubility of the liquid state is exceeded, the melting of the laser causes the degassing of nitrogen. Due to the high cooling rate, the melt rapidly solidifies, and nitrogen is entrapped in the cooled material causing an increase in porosity in addition to other process-induced defects as found in Batch A.

Mechanical properties of L-PBF-built samples. For every batch, the averaged curves of three samples tested in the as-built as well as the T and QT conditions are depicted in Figure 8a and b, showing the compressive stress-compression curves. An exemplary sample after the compression test can be found in Figure 2c. As can be seen for Batch A, the specimens in the as-built condition exceed the strength of both the T and QT condition, while both heat-treated conditions show identical deformation behavior under the compressive load. For Batch B, another compression behavior was determined. The slope in the elastic region for the as-built condition is significantly lower, not only compared to Batch A but also to the T and QT condition of Batch B. A possible explanation for this may be a high implementation of dislocations during L-PBF and the corresponding rapid cooling as proposed by Benito et al. [23]. This behavior is completely reverted after both heat treatments conducted and resulting in a similar but recognizably increased elastic behavior with regard to the as-built state.

By comparison, the compressive strength at a plastic deformation of 0.2, 2, 10 and 20 % were plotted in Figure 9, including standard deviation, where the compressive strength at 0.2 % deformation corresponds to the compressive yield stress. Except for the compressive yield stress of the as-built condition of Batch B, all specimens with increased nitrogen content exceed the values of the raw material. By calculating the ratio of the compressive strength at 10 % and 20 % plastic deformation, it is possible to characterize the strain-hardening during the compression test. As can be seen in Figure 9a and b, the strain-hardening of the heat treated specimens for both batches is similar. The ratio calculated for these conditions is 1.07, while it is 1.11 and 1.22 for Batch A and B (as-built), respectively, confirming the higher strain-hardening behavior.

The different strain-hardening behavior in the as-built conditions for both batches can be explained by an incomplete transformation of austenite to martensite as described by Holzweissig et al. [24] due to the melting of overlying powder layers and a constant heat flow so that the material possibly does not reach the martensite-finish-

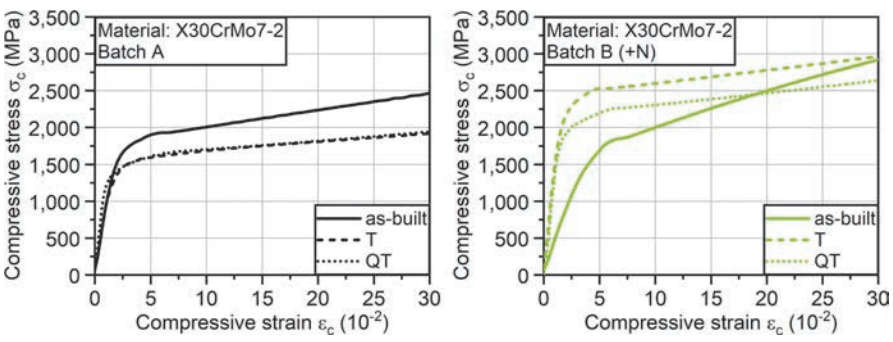

Figure 8: Compressive stress-strain curves for a) batch A and b) batch B

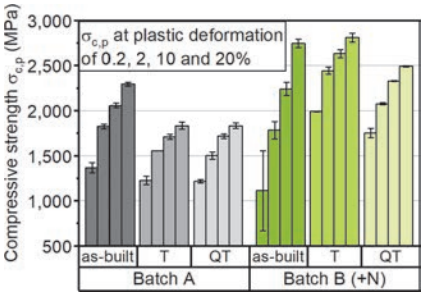

Figure 9: Compressive strength at defined plastic deformation of 0.2, 2, 10 and 20 % for batch A and B

temperature. During compression, the austenite retained can transform into martensite, which is even more pronounced for Batch B, where nitrogen stabilizes the austenitic phase [9, 10], preventing martensite formation during cooling and resulting in a significantly increased hardening behavior. The higher compressive strength for Batch B (T and QT) may also be related to the additional nitrogen, due to the effective strengthening of interstitial nitrogen [7], as most of the nitrides can dissolve in the matrix during austenitization [10]. The solid-dissolved nitrogen can lead to a more pronounced lattice distortion, which is an important aspect in solution strengthening. Furthermore, nitrogen enhances secondary hardening, resulting in higher hardness after tempering. The enhanced hardenability may be a result of a refinement of secondary precipitates that form from the martensite during tempering, which is a direct result of an ordering effect of nitrogen on the element distribution in the austenitic phase before martensitic transformation [22].

Conclusions

From the results presented, some conclusions can be drawn:

- Gas nitriding of X30CrMo7-2 steel powder using N_2 gas as a nitrogen donor at a comparably low temperature of 675 °C leads to a considerable nitrogen uptake. The low thermal dissociation rate is compensated for by the high specific surface of the powder.
- Due to the low nitriding temperature, sintering only marginally occurs and the flow properties of the steel powder after nitriding are comparable to the properties of the untreated powder.
- L-PBF processing of nitrided X30CrMo7-2 steel powder is possible. The high nitrogen content of the powder investigated exceeds the maximum solubility of the steel in liquid state, however, and thus results in a pronounced pore formation.
- Both heat treatments (tempering, quenching and tempering) decrease the hardness and compressive yield stress of the raw material from 1,366 MPa to 1,225 and 1,216 MPa, respectively. Tempering increases the compressive yield stress of the specimens with nitrogen significantly rising from 1,111 MPa to 1,990 MPa as compared to the as-built condition, while quenching and tempering combined result in a less pronounced increase reaching 1,752 MPa.
- The highest strain hardening behavior under compression can be found for both batches in the as-built condition. The addition of nitrogen even further increases strain hardening, whereas after both heat treatments conducted, this behavior decreased and no significant differences in strain hardening could be observed.

Acknowledgement

The authors would like to thank the German Research Foundation (DFG) for its financial support within the scope of the research project “Mechanism-based assessment of the influence of powder production and process parameters on the microstructure and the deformation behavior of SLM-compacted C+N steel in air and in corrosive environments“ (WA 1672/30-1, TH 531/20-1 and ZO 140/22-1) as well as A. Schulz, V. Uhlenwinkel and H.-W. Zoch (Leibniz Institute for Materials Engineering, Bremen) for the excellent scientific collaboration.

References

1 D. Bourell, J. P. Kruth, M. Leu, G. Levy, D. Rosen, A. M. Beese, A. Clare: Materials for additive manufacturing, CIRP Annals 66 (2017) 2, pp. 659-681 DOI:10.1016/j.cirp.2017.05.009

2 D. Gu, Z. Wang, Y. Shen, Q. Li, Y. Li: In-situ TiC particle reinforced Ti–Al matrix composites: Powder preparation by mechanical alloying and selective laser Melting behavior, Applied Surface Science 255 (2009), No. 22, pp. 9230-9240 DOI:10.1016/j.apsusc.2009.07.008

3 B. AlMangour, D. Grzesiak, J.-M. Yang: Nanocrystalline TiC-reinforced H13 steel matrix nanocomposites fabricated by selective laser melting, Materials & Design 96 (2016), pp. 150-161 DOI:10.1016/j.matdes.2016.02.022

4 J. T. Sehrt, S. Kleszczynski, C. Notthoff: Nanoparticle improved metal materials for additive manufacturing, Progress in Additive Manufacturing 2 (2017), No. 4, pp. 179-191 DOI:10.1007/s40964-017-0028-9

5 C. Doñate-Buendía, F. Frömel, M. B. Wilms, R. Streubel, J. Tenkamp, T. Hupfeld, M. Nachev, E. Gökce, A. Weisheit, S. Barcikowski, F. Walther, J. H. Schleifenbaum, B. Gökce: Oxide dispersion-strengthened alloys generated by laser metal deposition of laser-generated nanoparticle-metal powder composites, Materials & Design 154 (2018), pp. 360-369 DOI:10.1016/j.matdes.2018.05.044

6 H. Springer, C. Baron, A. Szczepaniak, E. A. Jägle, M. B. Wilms, A. Weisheit, D. Raabe: Efficient additive manufacturing production of oxide- and nitride-dispersion-strengthened materials through atmospheric reactions in liquid metal deposition, Materials & Design 111 (2016), pp. 60-69 DOI:10.1016/j.matdes.2016.08.084

7 J. W. Simmons: Overview: high-nitrogen alloying of stainless steels, Materials Science and Engineering A 207 (1996), No. 2, pp. 159-169 DOI:10.1016/0921-5093(95)09991-3

8 T. Biggs, R. D. Knutsen: The effect of nitrogen on martensite formation in a Cr-Mn-Ni stainless steel, Le Journal de Physique IV 05 (1995), No. C8, pp. 515-520 DOI:10.1051/jp4 : 1995879

9 X. P. Ma, L. J. Wang, B. Qin, C. M. Liu, S. V. Subramanian: Effect of N on microstructure and mechanical properties of 16Cr5Ni1Mo martensitic stainless steel, Materials & Design 34 (2012), pp. 74-81 DOI:10.1016/j.matdes.2011.07.064

10 J. Gu, J. Li, Y. Chen: Microstructure and strengthening-toughening mechanism of nitrogen-alloyed 4Cr5Mo2 V hot-working die steel, Metals 7 (2017) 310, pp. 1-14 DOI:10.3390/met7080310

11 H. Hänninen, J. Romu, R. Ilola, J. Tervo, A. Laitinen: Effects of processing and manufacturing of high nitrogen-containing stainless steels on their mechanical, corrosion and wear properties, Journal of Materials Processing Technology 117 (2001), pp. 424-430 DOI:10.1016/S0924-0136(01)00804-4

12 H. J. Grabke: High Nitrogen Steels. The role of nitrogen in the corrosion of iron and steels, ISIJ International 36 (1996), No. 7, pp. 777-786 DOI:10.2355/isijinternational.36.777

13 J. Menzel, W. Kirschner, G. Stein: High Nitrogen Steels. High nitrogen containing Ni-free austenitic steels for medical applications, ISIJ International 36 (1996), No. 7, pp. 893-900 DOI:10.2355/isijinternational.36.893

14 C. Duan, Y. Shen, X. Feng, C. Chen, J. Zhang: Nitriding of Fe–18Cr–11Mn powders using mechanical alloying method through aerating nitrogen circularly, Materials Science and Technology 32 (2016); No. 12, pp. 1231-1239 DOI:10.1080/02670836.2015.1115244

15 C. Duan, C. Chen, J. Zhang, Y. Shen, X. Feng: Nitriding of Fe–18Cr–8Mn stainless steel powders by mechanical alloying method with dual nitrogen source, Powder Technology 294 (2016), pp. 330-337 DOI:10.1016/j.powtec.2016.02.048

16 T. Nakamoto, N. Shirakawa, N. Ueda, Y. Miyata, T. Sone: Plasma nitriding to selective laser sintering parts made of SCM430 powder, Surface and Coatings Technology 202 (2008), No. 22-23, pp. 5484-5487 DOI:10.1016/j.surfcoat.2008.06.095

17 J. Boes, A. Röttger, C. Mutke, C. Escher, W. Theisen: Microstructure and mechanical properties of X65MoCrWV3-2 cold-work tool steel produced by selective laser melting, Additive Manufacturing 23 (2018), pp. 170-180 DOI:10.1016/j.addma.2018.08.005

18 J. Krell, A. Röttger, K. Geenen, W. Theisen: General investigations on processing tool steel X40CrMoV5-1 with selective laser melting, Journal of Materials Processing Technology 255 (2018), pp. 679-688 DOI:10.1016/j.jmatprotec.2018.01.012

19 W. Schatt: Pulvermetallurgie: Technologien und Werkstoffe, 2nd Ed., Springer, Berlin, Germany (2007)

20 H. Berns, W. Trojahn, H.-W. Zoch: On the benefits of nitrogen in bearing steels, Ascometal (Ed.): Proc. of the 3rd Ascometal Bearing Steels Symposium, Arles-sur-Rhône, France (2000), pp. 119-123
21 D. Junker, O. Hentschel, M. Schmidt, M. Merklein: Investigation of heat treatment strategies for additively-manufactured tools of X37CrMoV5-1, Metals 8 (2018), 854, pp. 1-13 DOI:10.3390/met8100854
22 V. G. Gavriljuk, H. Berns: High Nitrogen Steels: Structure, Properties, Manufacture, Applications, Springer, Berlin, Germany (1999)
23 J. A. Benito, J. Jorba, J. M. Manero, A. Roca: Change of Young's modulus of cold-deformed pure iron in a tensile test, Metallurgical and Materials Transactions A 36 (2005), No. 12, pp. 3317-3324 DOI:10.1007/s11661-005-0006-6
24 M. J. Holzweissig, A. Taube, F. Brenne, M. Schaper, T. Niendorf: Microstructural characterization and mechanical performance of hot work tool steel processed by selective laser melting, Metallurgical and Materials Transactions B 46 (2015), No. 2, pp. 545-549 DOI:10.1007/s11663-014-0267-9

Bibliography

DOI 10.3139/120.111446
Materials Testing
62 (2020) 1, pages 19-26

ISSN 0025-5300

The authors of this contribution

MSc Felix Stern, born in 1991, studied Nano- and Material Science at the Westphalian University of Applied Sciences, Recklinghausen, Germany, and received his Bachelor's degree in 2014. In 2017 he successfully completed his Master's degree in Material Science and Engineering at the University of Siegen, Germany. Since then, he has been working as a research assistant at the Department of Materials Test Engineering at TU Dortmund University. His main research topic is the mechanical characterization of additively manufactured steel with a focus on fatigue behavior.

BSc Felix Grabienski, born in 1995, studies Mechanical Engineering at TU Dortmund University, Germany. In his Bachelor's thesis he characterized the influence of the increased nitrogen content on the mechanical properties of additively manufactured tool steel X30CrMo7-2.

Prof. Dr.-Ing. Frank Walther, born in 1970, studied Mechanical Engineering, majoring in Materials Science and Engineering at TU Kaiserslautern University, Germany. There, he completed his PhD on the fatigue assessment of railway wheel steel in 2002 and his habilitation on physical measurement techniques for microstructural-based fatigue assessment and lifetime calculation of metals in 2007. At Schaeffler AG in Herzogenaurach, Germany, he was in charge of Public Private Partnership within Corporate Development from 2008 to 2010. Since 2010 he has been Professor for Materials Test Engineering (WPT) at TU Dortmund University, Germany. His research portfolio includes determination of process-structure-property-damage relationships of metal- and polymer-based materials and components under fatigue loading from the LCF to VHCF range, taking into account the influence of manufacturing and joining processes as well as service loading and corrosion deterioration.

MSc Johannes Boes, born in 1990, studied Mechanical Engineering at Ruhr University Bochum, Germany, specializing in Material Science and Technology and received his Master's degree in 2016. Since then, he has been working as a Research Assistant at the Chair for Materials Technology at Ruhr University Bochum. His research focuses on the development of new high alloyed steel for laser additive manufacturing.

Dr.-Ing. Arne Röttger, born in 1983, studied Mechanical Engineering at the Fachhochschule Südwestfalen Abteilung Soest, Germany, specializing in Apparatus and Plant Engineering and received his Diploma in 2004. Additionally, he received a Diploma at Ruhr University Bochum, Germany, in 2007 in Mechanical Engineering, specializing in Materials Technology. From 2008 to 2011, he worked as a Research Assistant at the Chair for Materials Technology at Ruhr University Bochum and finished his PhD thesis in 2011. Since 2012, he has been a group leader at the Chair for Materials Technology at Ruhr University Bochum. His research focuses on resource-saving technologies in the field of the production and application of Fe- and Co-based materials, such as tool steel, metal-matrix-composites and hard alloys.

Prof. Dr.-Ing. Werner Theisen studied Mechanical Engineering at Ruhr University Bochum, Germany. After receiving his diploma in 1984, he started working as a Research Assistant at the Chair for Materials Technology at Ruhr University Bochum and finished his PhD thesis in 1988. He continued working at the Chair for Materials Technology as Chief Engineer and habilitated in 1996. From 1996 to 2000, he headed the department "Technology" at the Maschinenfabrik Köppern GmbH & Co. KG in Hattingen, Germany. Since 2000, he has been Professor for Materials Technology at Ruhr University Bochum. His research interests concentrate on the development and optimization of parts, fundamental relations between the microstructure and properties of materials during fabrication and application, alloy development and wear characterization. In this context, tool steels, nitrogen-alloyed steels, Fe-, Ni- or Co-based hard alloys and metal-matrix-composites, as well as Ni-Ti shape memory alloys are at the focus of his research.